PCCP

ROYAL SOCIETY OF CHEMISTRY

PAPER

View Article Online
View Journal | View Issue

Cite this: *Phys. Chem. Chem. Phys.*, 2024, **26**, 18435

Stability, electronic properties and CO adsorption properties of bimetallic PtAg/Pt(111) surfaces†

Luis A. Mancera, Axel Groß and R. Jürgen Behm *

Received 22nd April 2024,
Accepted 10th June 2024

DOI: 10.1039/d4cp01640h

rsc.li/pccp

Aiming at a better fundamental understanding of the chemistry of bimetallic PtAg/Pt(111) surfaces, we have investigated the stability, electronic properties and CO adsorption properties of bimetallic PtAg surfaces, including pseudomorphic Ag film covered Pt(111) surfaces and Pt_xAg_{1-x}/Pt(111) monolayer surface alloys, using periodic density functional theory calculations. The data provide detailed insights into the relative stabilities of different surface configurations, as indicated by their formation enthalpies and surface energies, and changes in their electronic properties, *i.e.*, in the projected local densities of states and shifts in the d-band center. The adsorption properties of different Pt_n ensembles were systematically tested using CO as a probe molecule. In addition to electronic ligand and strain effects, we were particularly interested in the role of different adsorption sites and of the local CO_{ad} coverage, given by the number of CO molecules per Pt surface atom in the Pt_n ensemble. Different from PdAg surfaces, variations in the adsorption energy with adsorption sites and with increasing local coverage are small up to one CO_{ad} per Pt surface atom. Finally, formation of multicarbonyl species with more than one CO_{ad} per Pt surface atom was tested for separated Pt_1 monomers and can be excluded at finite temperatures. General trends and aspects are derived by comparison with comparable data for PdAg bimetallic surfaces. Fundamental insights relevant for applications of bimetallic Pt catalysts, specifically PtAg catalysts, are briefly discussed.

1. Introduction

Bimetallic surfaces and catalysts have attracted considerable interest over recent decades, both for fundamental reasons, but in particular because of the attractive catalytic properties of bimetallic catalysts, which were often found to exceed the performance of their constituents in terms of activity, selectivity and stability.[1–6] The improved catalytic performance was attributed to an interplay of a number of different effects such as geometric ensemble effects, electronic ligand effects and electronic strain effects, where the first describes the influence of the size/configuration of active surface ensembles.[7,8] Electronic ligand effects describe the effect of electronic modifications of the active site by different neighboring surface atoms.[9,10] These as well as strain effects, which reflect the effect of lattice distortions as compared to the natural lattice of the respective surface layer on the electronic structure,[11] can lead to changes in the adsorption energy and thus to significant modifications in the reaction kinetics.[12,13] Finally, site-blocking effects, which reduce the number of active sites, have to be considered as well.[14–16] Initially, these different effects were mainly derived from changes in the catalytic activity upon varying the concentration of the respective components. More direct studies of these effects, correlating structural and electronic modifications with catalytic properties, became feasible with the advent of modern high-resolution spectroscopies and microscopies and in particular of theoretical methods, in combination with the increasing knowledge of the reproducible preparation of structurally well-defined model surfaces/systems.[17,18]

As part of an extensive series of combined experimental and theoretical studies on the structure, stability, electronic properties and adsorption behavior of structurally well-defined bimetallic PdAg/Pd(111)[18–23] and PtAg/Pt(111)[24–28] surfaces, we here report results of a theoretical study on the stability of different Ag/Pt(111) and PtAg/Pt(111) surfaces, as indicated by the formation enthalpy and surface energies, on their electronic properties, and on the CO adsorption behavior.

The structure, formation and stability of PtAg/Pt(111) surface alloys have been characterized previously using a variety of different techniques,[29–32] and the results were summarized previously by Jankowski *et al.*[33] and by Bauer *et al.*[34] These studies found that deposition of submonolayer amounts of Ag on Pt(111) and subsequent annealing to about 620 K result in the formation of monolayer PtAg surface alloys, where the Ag atoms are confined to the topmost layer[24,29,30,32] with a tendency to phase separation to form two-dimensional, homoatomic ensembles rather than a random distribution.[25] Thermal

Institute of Theoretical Chemistry, Ulm University, Oberberghof 7, D-89081 Ulm, Germany. E-mail: juergen.behm@uni-ulm.de

† Electronic supplementary information (ESI) available. See DOI: https://doi.org/10.1039/d4cp01640h

and CO induced intermixing of Pt and Ag in Ag films on Pt(111) and in Pt film covered Ag(111) surfaces were investigated by Jankowski *et al.*[33] experimentally and by Hua *et al.* theoretically.[35] Thermodynamically, none of these structures are stable because of entropic reasons. It depends on the reaction conditions whether these structures are kinetically stable. For the oxygen reduction reaction, our earlier work demonstrated that they are stable at room temperature.[27,28]

Most important for the present study is the finding of a pronounced ligand effect, with neighboring Ag surface atoms, leading to strengthening of the Pt–CO bond, due to an increased back-donation from the Pt atom into the $2\pi^*$ orbital of the adsorbed CO. Counteracting effects resulting from the compressive strain, due to the larger size of the Ag atoms and the pseudomorphic growth of the surface alloy, seemed to be less important. These experimental results, which were based mainly on temperature-programmed desorption (TPD) and infrared spectroscopy (FTIR) results, were also supported by DFT calculations.[25] Furthermore, the authors reported distinct changes in the adsorption site on these surface alloys with increasing CO_{ad} coverage, which also depended on the Ag surface concentration and thus on the relative concentration of small ensembles such as Pt_1 monomers, Pt_2 dimers, compact Pt_3 trimers and larger Pt_n ensembles.[25] A later high-resolution XPS study, which could also distinguish bridge-bonded CO from on-top adsorbed CO based on their slightly different C 1s binding energies, essentially confirmed these findings.[34]

These bimetallic surfaces can be considered as model systems for realistic bimetallic systems, which because of their well-defined and simple structure can provide detailed information on the structural and electronic effects on the surface chemistry of bimetallic surfaces that is not easily accessible from realistic systems. The closest realistic analogue to PtAg surface alloys and Ag film covered Pt surfaces may be Pt–Ag core–shell particles, which have been investigated as bimetallic catalysts in different reactions.[36–38]

In the present study, we are particularly interested in identifying possible highly stable local structures and in correlations between the electronic properties of specific Pt_n ensembles and their CO adsorption strength. Considering the CO adsorption behavior we are most interested in changes in the adsorption characteristics with increasing local coverage, *i.e.*, with an increasing number of CO_{ad} per Pt surface atom in Pt_n ensembles in bimetallic surfaces. This expands on our earlier report, where we explored the low-coverage CO adsorption behavior on small Pt_n ensembles (n = 1–3) in Pt_xAg_{1-x}/Pt(111) monolayer surface alloys, with 1 CO molecule per Pt_n ensemble.[25] Studies of the high-coverage regime are particularly interesting, since adsorption on spatially separated Pt ensembles may allow local coverages that are not accessible on an active smooth surface such as low-index single-crystal Pt surfaces, where saturation CO_{ad} coverages are in the order of 0.7 monolayers.[39,40] As an extreme example, multicarbonyl species with more than one CO bound to a Pt atom were proposed by Tsang *et al.* and Oduro *et al.* for Co-doped Pt catalysts.[41,42] Combining the present data with earlier results,[25,34] we will also try to obtain further information on the role of electronic ligand and strain effects. Finally, aiming also at a more general understanding, we will compare the results obtained here with comparable data reported earlier for a structurally rather similar PdAg/Pd(111) system.[23]

2. Computational details

Plane-wave DFT calculations were performed using version 5.3.3.4 of the VASP code,[43] together with the Perdew–Burke–Ernzerhof (PBE)[44] and the revised-PBE (RPBE)[45] exchange–correlation functionals. The ionic cores are represented by projector augmented wave (PAW) potentials[46] as constructed by Kresse and Joubert.[47,48] The electronic one-particle wave functions are expanded in a plane-wave basis set up to a cutoff energy of 400 eV. This cutoff energy, which corresponds to the maximum cutoff for the four atomic species considered in this study (Pt, Ag, C, and O) and is larger than the default values preset in the code for platinum and silver, was set manually in order to keep it constant for all calculations. Default cutoff energies are already expected to provide convergence better than 1 mRy ($\sim$13 meV) in eigenvalues for this kind of basis set. Spin polarization is not considered due to the non-spin-polarized nature of the system. Dipole moment correction is set up in order to account for effects derived from using asymmetric slabs. Scalar relativistic effects are already included from the parametrization at the basis set generation. Convergence criteria for the electronic self-consistency and the ionic relaxation were set to 1×10^{-5} eV and 1×10^{-4} eV, respectively. A sufficiently large set of k-points was chosen in order to guarantee convergence.

First, the bulk energies (E_b) and bulk lattice parameters (d_b) of Pt and Ag were computed using an fcc unit cell and a $11 \times 11 \times 11$ Γ-centered k-point grid. Values obtained using PBE/PAW for the bulk lattice parameter are 3.97 Å and 4.15 Å for Pt and Ag, respectively. These are in close agreement with the experimental values of 3.9231 Å and 4.0862 Å.[49] This yields nearest-neighbor distances of $d_s = \frac{\sqrt{2}}{2} d_b$ of 2.81 Å and 2.93 Å for Pt(111) and Ag(111), respectively, which in the following we denote as surface lattice parameters. Using RPBE, the bulk lattice parameters for Pt and Ag are 3.99 Å and 4.21 Å, respectively, and the nearest-neighbor distances for Pt(111) and Ag(111) are 2.82 Å and 2.98 Å, respectively. Note that RPBE yields a slightly larger overestimation of these parameters than PBE compared with the experimental values, as is well known for many systems.[50]

The bimetallic surfaces are represented by periodic slabs consisting of five monolayers. The vertical height of the three-dimensional unit cell was set to an integer multiple of the surface lattice parameter, $10d_s$, which allows us to have a separation between slabs close to 18 Å in all cases. Geometry optimization of the various surface configurations was carried out keeping the two bottom Pt(111) layers fixed at their corresponding bulk positions, while the three upper layers were allowed to relax. We used a (3×3) surface unit cell and

performed geometry optimizations using a $3 \times 3 \times 1$ Γ-centered k-point grid. For the various structures studied here we used the following notation: $Ag_{n}L/Pt(111)$ denotes a structure with n pseudomorphic silver overlayers above the Pt(111) substrate, $Pt_{1-x}Ag_x/Pt(111)$ denotes a surface alloy in the topmost layer, and $Pt_{1-x}Ag_x/Ag_{n}L/Pt(111)$ denotes a structure with a surface alloy at the topmost overlayer and n pseudomorphic Ag layers underneath. These structures will later in the paper be abbreviated as Pt_{5L} (= Pt(111)), Ag_{1L}/Pt_{4L} ($Ag_{1L}/Pt(111)$), $PtAg_{1L}/Pt_{4L}$ ($PtAg_{1L}/Pt(111)$) *etc.* Finally, we would like to add that because of the similarity in these calculations we expect relative energy changes by 0.01 eV to be significant, both for formation enthalpies and adsorption energies.

3. Results and discussion

3.1. Stability of silver/platinum bimetallic surfaces

The stability of the bimetallic surfaces was mainly characterized by their formation enthalpies. The formation enthalpies (ΔH) of the bimetallic surfaces were calculated according to Barabash *et al.*[51] Starting from the Pt(111) surface, we obtain

$$\Delta H = E_{Ag_{n}L/Pt(111)} - E_{Pt(111)} - x(E_{Ag} - E_{Pt}), \qquad (1)$$

for the layered systems, where $E_{Ag_{n}L/Pt(111)}$ and $E_{Pt(111)}$ are the total energies of the $Ag_{n}L/Pt(111)$ and Pt(111) slabs per surface atom, respectively. x denotes the fraction of Pt atoms replaced by Ag atoms in the slab relative to the number of surface atoms, E_{Ag} and E_{Pt} are the bulk energies per atom of these metals, and ΔH represents the mean formation enthalpy per surface atom. Note that this means that x can be larger than one, *e.g.*, in those systems where the topmost 2 or 3 Pt layers are replaced by Ag. This equation can also be used for the monolayer surface alloys, where exchange occurs only in the topmost layer. Hence, ΔH describes the energy difference per surface atom between the final $Ag_{n}L/Pt(111)$ or $Pt_{1-n}Ag_n/Pt(111)$ slab and the pure Pt(111) slab, after replacing some Pt (surface) atoms with Ag atoms moved to/taken from the respective bulk reservoirs. Physically, this approach with using Pt(111) as a reference is justified by the fact that the bimetallic systems explored in this study contain Pt(111) bottom layers. Hence, ΔH describes the energy required/released upon replacing part of the upper layers of the Pt(111) slab by Ag atoms. In contrast, for monometallic slabs such as Ag(111) or laterally compressed Ag(111) slabs the choice of the reference material is arbitrary, and therefore these numbers would have little meaning and are not provided.

We also calculated surface energies *via* the relationship in eqn (2)

$$E_S = \frac{1}{2A}\left(E_{slab} - \sum_i n_i E_i\right) \qquad (2)$$

where E_{slab} is the total energy of the slab, n_i denotes the number of atoms of type i in the slab (per unit cell), E_i denote the bulk energies (per atom) of these species, and A is the surface area of the unit cell. However, surface energies calculated this way represent an average of the surface energies of the upper and lower side of the slab, which are not necessarily the same in our study. Furthermore, these surface energies also contain contributions from the energy of the internal interface between Pt and Ag (interface energy). To avoid the first problem, we will also provide estimated surface energies of the Ag containing surfaces, which were calculated from the value calculated *via* eqn (2) by assuming that the surface energy of the bottom side is identical with that of a Pt(111) surface, which seems to be reasonable. Nevertheless, we will base our discussion of the stability of the different surface configurations mainly on the formation enthalpies and use surface energies only for comparison of rather similar surfaces, such as the Ag film covered surfaces. We would also like to note that while both surface energy and formation enthalpy represent measures of the stability, the references are different. The surface energy, often defined as the energy per surface area required to cleave an infinite crystal along a certain orientation, reflects the driving force towards reducing the surface area, *e.g.*, by sintering, and also the tendency of a given component to accumulate at the surface, *e.g.*, by surface segregation. The formation enthalpy indicates the enthalpy gained upon formation of the respective slab, as compared to the bulk energies of the separate components. Hence, it also indicates the tendency for phase separation. For the following it is important to keep in mind that in all calculations the Pt atoms in the bottom most two layers are fixed on their bulk positions and not allowed to relax vertically, providing a structurally adequate model of a Pt(111) substrate. For surface energies, which are determined by the breaking of bonds that are three layers away from the bottom two layers, deviations caused by the limited thickness of the Pt substrate part, will be negligible. For CO adsorption energies, which are mainly determined by the direct neighborhood of the adsorbed molecule, we expect the same. For the enthalpies of formation, there may be small deviations in the absolute values of the formation enthalpies due to the limited thickness of the Pt(111) bulk representation, but the differences in formation enthalpies of different configurations and thus the general trends between different structures are expected to be fully correct.

3.1.1. $Ag_{n}L/Pt(111)$ pseudomorphic overlayers. Table 1 shows both formation enthalpies and surface energies calculated using PBE/PAW and RPBE/PAW. Here we find the most negative formation enthalpies (highest stability) for the Ag film covered surfaces, with minute differences between different Ag film thicknesses. Obviously, the costs for surface and interface formation vary very little with Ag film thickness. For the Pt-terminated surfaces, the formation energies are close to zero, *i.e.*, the presence of the Ag underlayer and the formation of the two internal Pt–Ag interfaces has little effect on the energetics of these systems as compared to Pt(111). For the monometallic Ag systems we do not provide formation enthalpies for reasons discussed in Section 3.1.

By and large, these trends are also reflected by the surface energies, with higher surface energies for less negative formation enthalpies. Among the Ag containing surfaces, those with Ag at the surface exhibit the lower surface energy. Hence,

Table 1 Formation enthalpies (ΔH), surface energies (E_S) and estimated surface energies of the top surface ($E_{S,top}$, see text) for pure Pt(111) and Ag(111) surfaces and for Ag_{nL}/Pt(111) pseudomorphic overlayers, varying the number of Ag layers (PBE/PAW). Surface energies and formation enthalpies are given in meV Å^{-2}. Ag_{5L}/Pt_{0L} denotes the pure Ag(111) surface, keeping the lateral lattice parameter of Pt(111), whereas Ag_{5L} denotes the pure Ag(111) surface with the Ag lattice parameter. Note the conversion: 1 meV Å^{-2} ≈ 16.02 × 10^{-3} J m^{-2}. For the systems with a Pt(111) lattice, 1 meV per surface atom corresponds to 0.1462 meV Å^{-2} for a slab of identical thickness. Results obtained *via* RPBE/PAW are shown in Table S1 in the ESI

Ensemble	ΔH	E_S	$E_{S,top}$
Pt_{5L}	0.0	100.5	100.5
Ag_{1L}/Pt_{4L}	−43.9	78.4	56.3
Ag_{2L}/Pt_{3L}	−43.9	78.3	56.1
$Pt_{1L}/Ag_{1L}/Pt_{3L}$	−21.9	89.3	78.1
Ag_{3L}/Pt_{2L}	−42.4	79.4	58.3
$Pt_{2L}/Ag_{1L}/Pt_{2L}$	+8.8	105.1	109.7
$Pt_{1L}/Ag_{2L}/Pt_{2L}$	−24.9	88.2	75.9
Ag_{5L}/Pt_{0L}	—	25.8	—
Ag_{5L}	—	47.5	—

Table 2 Mean enthalpies of formation (upper lines), differential enthalpies of formation (middle lines), and surface energies (bottom lines), for the PtAg/Ag_{nL}/Pt(111) surface alloys indicated. Surface energies and formation energies are given in meV Å^{-2} (1 meV Å^{-2} ≈ 16.02 × 10^{-3} J m^{-2}). For the systems with a Pt(111) lattice, 1 meV per surface atom corresponds to 0.1462 meV Å^{-2} for a slab of identical thickness. Results were obtained using PBE/PAW, and data using RPBE/PAW are collected in Table S2 in the ESI

		Pt_1	Pt_2	Pt_3	Pt_4
Ensemble	θ_{Pt}	1/9	2/9	3/9	4/9
PtAg/Pt_{4L}	ΔH	−38.0	−33.6	−27.8	−21.9
	ΔH_{diff}	−38.0	−29.2	−16.1	−4.4
	E_S	81.2	83.7	86.7	89.3
PtAg/Ag_{1L}/Pt_{3L}	ΔH	−43.9	−43.9	−45.3	−43.9
	ΔH_{diff}	−43.9	−43.9	−48.2	−39.5
	E_S	78.5	78.2	77.8	78.6
PtAg/Ag_{2L}/Pt_{2L}	ΔH	−39.5	−36.6	−36.6	−35.1
	ΔH_{diff}	−39.5	−33.6	−36.6	−30.7
	E_S	80.8	81.9	82.5	83.3

as expected, the termination by Ag (plus the formation of the Pt–Ag interface) is more favorable than Pt termination. Note that the estimated surface energies of the top layer of the Ag-terminated surfaces differ only little from that of Ag(111). On the other hand, contributions from interface energies are likely responsible for the high value of the surface energy of $Pt_{2L}/Ag_{1L}/Pt_{2L}$, which is even higher than that of Pt(111).

Interestingly, these trends differ significantly from those obtained for comparable Ag_{nL}/Pd(111) systems.[23] While for Ag_{nL}/Pt(111) surfaces the surface energies/formation enthalpies are approximately identical for films with 1, 2 or 3 pseudomorphic Ag layers, there are significant differences for Ag_{nL}/Pd(111) film surfaces, with a distinct increase of the surface energy/decrease of the formation enthalpy from the first to the second Ag layer film, while for the 3 layer system the changes are small. We do not have a specific explanation for this trend, but we like to note that in spite of the fact that Pt is situated below Pd in the periodic table, there are many differences in the chemical properties of these two elements, for example with respect to their CO adsorption properties. This shall be investigated in more detail in the future.

Finally, we would like to note that all calculations were performed for pseudomorphic overlayer systems, even though experimentally only Ag monolayer films remain pseudomorphic, while for bilayer and thicker films strain relief results in the formation of a unidirectionally expanded (striped) phase or, upon annealing, in a trigonal incommensurate phase, where strain is relieved isotropically.[52,53] Despite these structural differences, the data derived here provide detailed insight in trends in the stability of the different configurations.

3.1.2. Pt_xAg_{1-x}/Pt(111) surface alloys. The formation enthalpies and the surface energies were evaluated also for Pt_xAg_{1-x}/Pt(111) monolayer surface alloys with compact Pt_1, Pt_2, Pt_3, and Pt_4 ensembles in the topmost layer, where these ensembles are separated from each other by Ag surface atoms. The smallest unit cell allowing this is a 3 × 3 unit cell. The ensembles correspond to the most compact structures, for example a triangle for Pt_3 and a rhombus for Pt_4. They are the result of substituting 8, 7, 6, or 5 Pt atoms by Ag atoms at the pure Pt(111) surface within the 3 × 3 unit cell, or equivalently, substituting 1, 2, 3, or 4 Ag atoms by Pt atoms in the pseudomorphic Ag monolayer in the Ag_{1L}/Pt(111) surface. These different ensembles allow the occupation of different types of CO adsorption sites such as on-top sites, bridge sites, threefold hollow sites, *etc.* Similar calculations were performed also for monolayer surface alloys supported on pseudomorphic Ag monolayer (PtAg/Ag_{1L}/Pt_{3L}) and bilayer (PtAg/Ag_{2L}/Pt_{2L}) films on the Pt(111) substrate. The results obtained for using PBE/PAW are collected in Table 2, and those for RPBE/PAW in Table S2 in the ESI.† Furthermore, the formation enthalpies are plotted in Fig. 1 as a function of the Ag content in the surface layer, including also higher Pt concentrations.

As shown in Table 2 and in Fig. 1, the formation enthalpy decreases almost linearly (becomes less negative) with increasing Pt content in the topmost layer for PtAg/Pt_{4L}. Conversely, it increases with increasing Ag content. In Fig. 1, the first (x = 0) and last (x = 1) point represent the values for the Pt(111) and $Ag_{1L}Pt_{4L}$ systems, respectively. The approximately linear decay of the mean formation enthalpy can be converted into a differential value, indicating the differential change in system energy upon exchanging another surface atom, which are also listed in Table 2. Here we see a more pronounced decay, reaching the zero level at n = 4. Consequences of these data with respect to the preferential formation of larger ensembles will be discussed later in this section. Finally, the surface energy increases with increasing Pt content in the surface layer, due to the stronger Pt–Pt bonds that have to be broken upon cleaving the crystal.

The PtAg/Ag_{1L}/Pt_{3L} surface alloys with a single Ag sublayer are noticeably more stable (more negative ΔH) than the PtAg/Pt_{4L} surface alloys. In Fig. 1, the first/last points correspond to the values of the Pt/Ag_{1L}/Pt_{4L} and the Ag_{2L}/Pt_{3L} systems, respectively. In this case, we find pronounced deviations from a strictly linear increase in the formation enthalpy, with almost

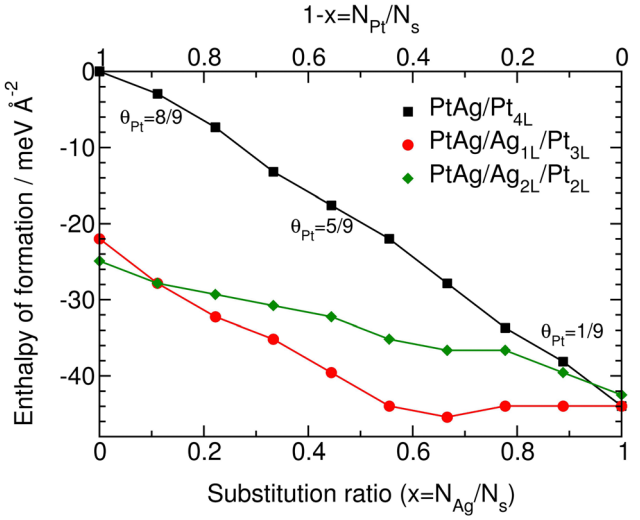

Fig. 1 Formation enthalpies ΔH in meV Å^{-2} for the $Pt_{1-x}Ag_x/Ag_{nL}/Pt(111)$ monolayer surface alloys as a function of the substitution ratio x. The index n_L denotes the number of pseudomorphic Ag layers between Pt(111) and the monolayer surface alloy, the substitution ratio x defines the number of Pt atoms replaced by Ag atoms in the topmost layer relative to the total number of surface atoms (here: 9). The $1 - x$ scale at the upper x-axis describes the fraction of Pt atoms in the topmost layer, which also corresponds to the Pt coverage Θ_{Pt} in the topmost layer. The results were obtained using PBE/PAW, for RPBE/PAW values see Fig. S1, ESI.†

constant values up to $n = 4$, followed by a slow increase. Actually, it looks like there is a minimum at $\Theta_{Pt} = 3/9$. Reasons for this very different behavior, also compared to the $PtAg/Ag_{2L}/Pt_{2L}$ system, can only be speculated upon in the moment. Also for the surface energy we find almost constant values for the Pt_1 monomer up to the Pt_4 tetramer ($x \geq 0.55$) (Table 2).

For the surface alloys with two Ag sublayers, we again find an almost linear relationship between the number of exchanged Pt surface atoms, but with a lower slope than for the $PtAg/Pt_{4L}$ surface alloys. In this case, the systems with $x = 0$ and $x = 1$ in Fig. 1 correspond to the $Pt_{1L}/Ag_{2L}/Pt_{2L}$ and Ag_{3L}/Pt_{2L} systems in Table 1, respectively. For a pure Ag surface layer ($x = 1$), all three surface alloys exhibit about the same formation enthalpy, which reflects the similar formation enthalpies of the $Ag_{nL}/Pt_{(5-n)L}$ systems with $n = 1$ to $n = 3$ (see Table 1). Except for the first and second data point, the formation energies are smaller (less negative) than for the $PtAg/Ag_{1L}/Pt_{3L}$ systems, and for all data points higher than for the $PtAg/Pt_{4L}$ surface alloys. The higher (more negative) values than for the $PtAg/Pt_{4L}$ surface alloys reflect a stronger bonding between Pt in the surface layer and Ag in the sublayer as compared to the mean value of the bulk energies (see eqn (1)). Apparently, this effect is more pronounced for the $PtAg/Ag_{1L}/Pt_{3L}$ than for the $PtAg/Ag_{2L}/Pt_{2L}$ system, which can be understood based on vertical ligand effects. Due to the stronger Ag–Pt bonding between the second and third layer (from the top) in $PtAg/Ag_{1L}/Pt_{3L}$ compared to Ag–Ag bonding in the other system, bonding between the Ag subsurface layer and the surface layer is relatively stronger in the $PtAg/Ag_{1L}/Pt_{3L}$ system. The lower slope compared to $PtAg/Pt_{4L}$ indicates that the energy gain per exchanged surface Pt, relative to the change in bulk energies, decreases less (more negative ΔH) with increasing Pt content than for the $PtAg/Pt_{4L}$ system. For $PtAg/Ag_{1L}/Pt_{3L}$, this effect is apparently in between the other two cases, and not linear. Finally, for the surface energy we find a slow increase from the Pt_1 monomer to the Pt_4 tetramer (Table 2).

For all systems considered, the surface alloys are stable with respect to phase separation (negative ΔH). Most stable is the $PtAg/Ag_{1L}/Pt_3$ system, although the differences between the different systems ($PtAg/Pt_{4L}$, $PtAg/Ag_{1L}/Pt_{3L}$, $PtAg/Ag_{2L}/Pt_{2L}$) are small. In a simple picture, one would expect a higher formation enthalpy for the $PtAg/Ag_{1L}/Pt_{3L}$ system compared to $PtAg/Pt_{4L}$, based on vertical ligand effects and bond order conservation, which is obviously not the case. Again, we expect this to result from contributions from the Pt–Ag interface(s). Using RPBE/PAW, there are no differences in the general trends (see Table S2, ESI†). There are some differences in individual results, but these are at the limit of the accuracy of the calculations.

Furthermore, these data also indicate a weak driving force for 2D clustering in the surface layer, in agreement with experimental findings.[25] As an example, the enthalpy gain obtained for creating a surface with 4 unit cells (area per unit cell: 61.56 Å^2) of Pt_1Ag_8/Pt_{4L} with a total ΔH of 4×61.56 Å^2 $\times$ -38.0 meV Å^{-2} = -9.36 eV is slightly lower than that for creating a surface with 3 unit cells of Ag_{1L}/Pt_{4L} (3×61.56 Å^2 $\times$ -43.9 meV Å^{-2} = -8.1 eV) plus one unit cell of Pt_1Ag_8/Pt_{4L} (61.56 Å^2 $\times$ -21.9 meV Å^{-2} = -1.35 eV), which yields in total -9.46 eV. Similar results are also obtained for other combinations.

These results can be compared with those obtained in a recent *in situ* microscopy study of alloying and de-alloying of Ag and Pt in Ag films on Pt(111)[33] and of a combined Monte Carlo and DFT study of segregation phenomena in Pt/Ag(111) systems.[35] Exploring the growth and alloying/dealloying behavior of Ag on Pt(111) at about 800 K, Jankowski *et al.* observed a complex dynamic behavior with increasing Ag deposition, confirming alloy formation in the first monolayer and subsequent dealloying at Ag coverages of more than 70% of a monolayer equivalent, by formation of monolayer islands with rather large Pt-rich central areas and Ag-rich rim areas.[33] The observation of PtAg monolayer surface alloy formation even at these temperatures underlines that this is not mainly due to kinetic limitations, but (largely) reflects thermodynamics. The large-scale 2D phase separation in the monolayer islands can hardly be compared with the present calculations due to the unknown composition of the original surface layer. Our calculations only covered the case of a surface layer on one or two Ag sublayers (see above), which is likely not the case in those experiments. Comparing the present results of a tendency towards monolayer surface phase separation with those reported by Hua *et al.*,[35] they do not seem to agree, since these authors arrived at high Pt_1 monomer surface concentrations for Pt/Ag(111) systems with low Pt bulk concentrations (<8%). In a more detailed look one has to keep in mind, however, that their simulation results were obtained for rather high temperatures, under dissolution – surface segregation equilibrium conditions, where phase separation is entropically disfavored. Furthermore, the formation of Pt_1 surface monomers was supported by CO

adsorption, which, as will be shown in Section 3.3, is strongest on Pt_1 monomers. Considering these aspects, there is no discrepancy to the present results for formation enthalpies and surface energies.

Finally, comparing these trends with those obtained for PdAg/Pd(111) surface alloys,[23] the general trends are very similar, but the effects of the Ag underlayer(s) are much more pronounced for PdAg/Pd(111) than for PtAg/Pt(111), which we tentatively attribute to differences in the interface effects.

In total, these data provide quantitative insights into the relative stabilities of different pseudomorphic surface configurations, starting from Ag film covered surfaces *via* surfaces terminated by one or two Pt(111) layers on one or two Ag underlayers *via* Pt_xAg_{1-x}/Pt(111) monolayer surface alloys to finally Pt_xAg_{1-x}/Pt(111) monolayer surface alloys supported on one or two Ag layers, all of them based on a Pt(111) substrate. They not only confirm the experimentally well-known tendency towards Ag termination of Ag containing surface regions, but also allow us to differentiate between different configurations. Furthermore, they also underline the need for improved calculations of the surface energy, where this is determined free from contributions from the bottom side of the slab.

3.2. Electronic properties of silver/platinum bimetallic surfaces

Since it is often used as a measure of the adsorption energy and therefore also of the chemical reactivity of catalyst surfaces, based on the d-band model and on the Sabatier principle,[54,55] we evaluated the local density of states (LDOS) on the Pt atoms in the topmost layer for the three surface alloys with Pt_1, Pt_2, and Pt_3 ensembles in the surface layer (Θ_{Pt} = 1/9, 2/9, 3/9), respectively, on the pure Pt_{4L} slab, and with one or two Ag sublayers in between. Fig. 2a shows the local DOS of the d-states projected on the Pt surface atoms in the pure Pt(111) surface and in the three corresponding surface alloys. Since this was already discussed in detail previously,[23] we here only summarize the main findings. While for the pure Pt(111) surface the center of the d-band is located at −2.07 eV, surface alloying with Ag leads to an upshift of the center of the d-band on the Pt atoms in the topmost layer, to −1.49 eV for Pt_1Ag_8, to −1.65 eV for Pt_2Ag_7 and to −1.72 eV for Pt_3Ag_6 (see Table 3). According to the d-band model, this upshift should correspond to an increase in CO adsorption energy on the Pt ensembles, which fully agrees with experimental findings.[25] Increasing the size of the Pt ensembles in the overlayer down-shifts the center of the d-band and brings it closer to that in pure Pt(111). Though not very big, these shifts are significant when compared with shifts reported for structural effects, *e.g.*, for steps[56] or for lattice strain effects.[11] The catalytic activity, in turn, would depend on the optimum adsorption strength for a given reaction. As an example, for the oxygen reduction reaction (ORR) the optimum oxygen adsorption strength was reported to be for a slightly weaker bonding than on Pt(111).[57] Hence, in that case the Pt_1Ag_8/Pt(111) sites would be less active than Pt(111) sites.

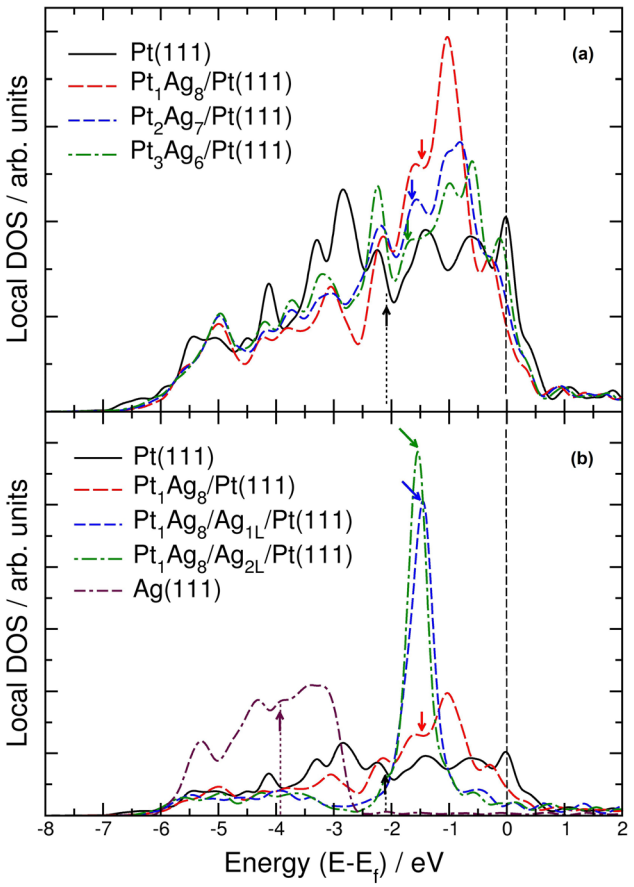

Fig. 2 Local density of d-states calculated by projection of the d-wave functions onto the atomic orbitals at a Pt top site (for Ag(111) on a Ag top site). In the upper box (a) we compare the pure Pt(111) surface and the PtAg/Pt_{4L} surface alloys containing Pt_1, Pt_2 and Pt_3 ensembles. All energies refer to the Fermi energy. Up-arrows denote the positions of the d-band centers for the Pt(111) surface and down-arrows denote the positions of the d-band centers for the surface alloys. In the lower box (b) we compare the LDOS at the Pt atom of PtAg surface alloys containing only Pt_1 monomers for different numbers of Ag underlayers (0, 1, 2, see figure). For comparison we also show projected LDOS for the pure Pt(111) and Ag(111) surfaces. Up-arrows denote the center of the band of the pure surfaces, while down-arrows denote the center of the band of the surface alloys. The results presented here were obtained using PBE/PAW.

This behavior is quite different to the trend in PdAg/Pd(111) surface alloys.[23] First of all, the shifts are much less

Table 3 Center of the d-band on the Pt surface atoms and relative shifts compared to Pt(111) in eV for different PtAg surface alloys. The results were obtained using PBE/PAW, and data using RPBE/PAW are collected in Table S3 in the ESI

Ensemble	d-band center	$\Delta_{\text{d-band center}}$
Pt(111)	−2.07	
Pt_1Ag_8/Pt_{4L}	−1.49	0.58
Pt_2Ag_7/Pt_{4L}	−1.65	0.42
Pt_3Ag_6/Pt_{4L}	−1.72	0.35
Pt_1Ag_8/Pt_{4L}	−1.49	
$Pt_1Ag_8/Ag_{1L}/Pt_{3L}$	−1.51	0.02
$Pt_1Ag_8/Ag_{2L}/Pt_{2L}$	−1.56	0.07
Ag(111)	−3.91	

pronounced for PdAg/Pd(111), where the center of the d-band on the Pd surface atoms is rather similar for Pd_1Ag_8, Pd_2Ag_7 and Pd_3Ag_6 systems, at about −1.34 eV, upshifted from the value for Pd(111) of −1.53 eV.[23] This leads to a maximum shift of the d-band center of about 0.2 eV, while for PtAg/Pt(111) it reaches up to 0.6 eV. Thus, Ag induced changes in the activity are expected to be much more pronounced for the PtAg/Pt(111) surface alloys than for PdAg/Pd(111), depending on the optimum adsorption strength and thus on the optimum position of the d-band center.

Next, we also evaluated the changes in the LDOS on the Pt atom in a Pt_1Ag_8 surface alloy upon varying the number of Ag underlayers from 0 to 2 (see Fig. 2b). The LDOS on a Ag atom in a Ag(111) surface is also included. Replacing the Pt subsurface layer with a Ag layer leads to a strong narrowing of the LDOS at the Pt atom at the surface, and the same effect is also observed for inserting 2 Ag layers. This kind of narrowing can be understood as a result of a weaker coupling of the Pt atom to the Ag subsurface layer as compared to the situation with no Ag layer underneath. Commonly, such effects are described as vertical ligand effects. Together with the narrowing of the LDOS, the center of the d-band shifts from 2.07 eV (Pt(111)) to −1.49 eV (Pt_1Ag_8/Pt(111)), −1.51 eV (Pt_1Ag_8/Ag_{1L}/Pt(111)) and −1.56 eV (Pt_1Ag_8/Ag_{2L}/Pt(111)) (see Table 3).

Comparing again with PdAg surface alloys,[23] the effects are again much smaller for these latter surface alloys, similar to the much smaller shifts observed upon varying the Pt or Pd ensemble size. Introducing one or two Ag underlayers for PtAg surface alloys shifts the center of the d-band by 0.02 and 0.07 eV, respectively, towards the Fermi level, while for PdAg surface alloys these shifts were 0.20 and 0.27 eV, respectively. Therefore, we expect also less pronounced changes in the binding energy of adsorbates to the Pd atom in the PdAg alloys with increasing number of Ag underlayers as compared to PtAg surface alloys. Finally, using RPBE/PAW we found the same trends for the shifts of the d-band center, which are listed in Table S3 in the ESI.†

The results presented in this section can at least qualitatively be understood in the following picture. Surface alloying a transition metal with a noble metal of larger size, while keeping the lattice constant in the pseudomorphic, topmost layer, leads to a competition between two effects: compressive strain because of the replacement of a smaller transition metal by a larger atom (strain effects) *vs.* the weaker interaction of the transition metal atoms with neighboring noble metal atoms (lateral ligand effects). In addition, structural effects, *e.g.*, the requirement of a certain minimum ensemble size (ensemble effects), may also play a role.[17] In contrast to PdAg/Pd(111) surface alloys, where these effects largely balance each other, and therefore cause only small shifts in the d-band center, ligand effects seem to be more dominant for PtAg/Pt(111) surface alloys. The weaker bonding to neighboring noble metal atoms results in an up-shift of the d-band center from Pt(111) to Pt_1Ag_8/Pt(111), followed by a back-shift with increasing number of Pt neighbors. Hence, while we expect strain effects to be of comparable magnitude for Pt and Pd based on their rather similar lattice parameters (3.9231 Å and 3.8898 Å, respectively[49]), ligand effects seem to be considerably stronger for PtAg/Pt(111) surface alloys than for PdAg/Pd(111) surface alloys. They dominate the modification in the electronic structure and thus also in the adsorption strength. Possible physical reasons for this discrepancy are currently being investigated in more detail.

In total, these data demonstrate subtle differences in the LDOS of the surface Pt atoms in the surface alloys, which we will later compare with the trends in the CO adsorption strength.

3.3. CO adsorption on Pt_xAg_{1-x}/Pt(111) surface alloys

In this section we will focus on specific aspects of CO adsorption that are relevant for studies of catalytic reactions under relevant reaction conditions,[58,59] but are often overlooked in model studies. This includes CO_{ad} coverage effects, *e.g.*, due to interactions between CO_{ad} molecules adsorbed at higher local coverages, both on small Pt_x ensembles and also on larger ensembles. As an extreme case, this also includes the formation of multicarbonyls, where more than 1 CO_{ad} is adsorbed per active (Pt) surface atom. Furthermore, we will explore proximity effects, *i.e.*, interactions between CO_{ad} on ensembles that are separated from each other by at least one Ag atom. In addition to the adsorption energies we also evaluated the adsorption geometry of the CO_{ad} species for additional structural information. Hence, this work expands on our previous study where we focused on low-coverage CO adsorption on PtAg/Pt(111) bimetallic surfaces.[25]

3.3.1. CO_{ad} coverage effects and CO_{ad}–CO_{ad} interactions on small Pt_n ensembles. First we will explore the effect of CO_{ad}–CO_{ad} interactions on CO adsorption on small Pt_n ensembles with n = 1–3 in PtAg/Pt(111) surface alloys. The CO_{ad} coverage is varied by stepwise addition of 1 CO per 3 × 3 unit cell, until full coverage with 1 CO_{ad} per Pt surface atom is reached. The resulting configurations are illustrated in Fig. 3, together with the corresponding adsorption energies and tilt angles. The tilt angles refer to the angle of the CO molecule relative to the surface normal, with positive values indicating a tilt away from a neighboring adsorbed CO, due to CO_{ad}–CO_{ad} repulsions, or away from a neighboring Pt surface atom. In addition to the mean adsorption energy per CO_{ad}, E_{ad}, we will also provide values for the differential adsorption energy $E_{ad,diff}$, as this is decisive for comparison with the experimentally determined activation energy for desorption or with the adsorption energies derived from adsorption isotherms. This is generally defined as $E_{ad,diff} = \frac{dE_{ad}}{d\theta}$, where dE_{ad} is the differential change in total adsorption energy and $d\theta$ is the differential increase in CO_{ad} coverage. In the present case, where the local CO_{ad} coverage is stepwise increased by 1 CO molecule per step, this changes to

$$E_{ad,diff} = \frac{\Delta E_{ad}}{\Delta n}, \quad (3)$$

where ΔE_{ad} is the change in total adsorption energy per unit cell and Δn is the increase in CO_{ad} molecules per unit cell, which is typically chosen to be Δn = 1 in the following examples.

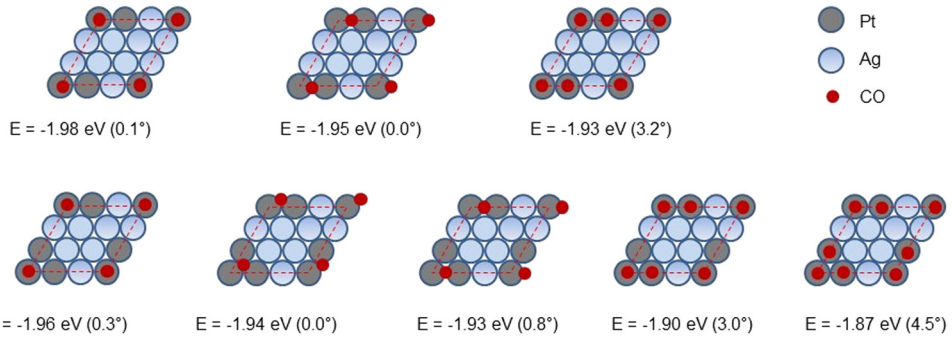

Fig. 3 Schematic representation of CO adsorption on different sites of Pt_1, Pt_2 and Pt_3 ensembles in Pt_1Ag_8/Pt(111), Pt_2Ag_7/Pt(111) and Pt_3Ag_6/Pt(111) surface alloys, respectively (energies in eV per molecule, angles refer to the tilt of the CO molecules with respect to the surface normal (see the text), for further details see the figure). Energies are calculated *via* PBE/PAW, and values obtained *via* RPBE/PAW are listed in the ESI† in Table S4.

The resulting data show the following trends: First, there is a trend toward increasing adsorption energies with increasing number of Ag neighbors (decreasing Pt ensemble size) in the low coverage limit (1 CO_{ad} per ensemble), even though the increase is rather small. Second, the differences between different adsorption sites are small, very much in contrast to previous findings of distinct ensemble effects for CO adsorption on Pd_n ensembles in PdAg/Pd(111)[20,23] and PdAu/Pd(111) surface alloys,[60–62] where the most favorable adsorption site changes from on-top for Pd_1 monomers to adsorption on Pd_2 bridge sites for Pd_2 dimers and finally Pd_3 threefold hollow sites on compact Pd_3 trimers. In contrast, for PtAg/Pt(111) adsorption on on-top sites is most favorable for Pt_1, Pt_2 and Pt_3 ensembles, although the differences are small for the latter two.[25]

While these trends were already reported previously,[25] we now furthermore find that there is also little difference in the adsorption energy per CO_{ad} molecule when increasing the CO_{ad} coverage, up to saturation of the respective Pt_n ensemble (1 CO_{ad} per Pt surface atom). Using PBE/PAW, going from a single 1 CO_{ad} to two CO_{ad} on a Pt_2 dimer changes the mean CO adsorption energy from −1.98 eV on on-top sites (−1.95 eV on bridge sites) to −1.93 eV, again on on-top sites. This corresponds to a change in the differential CO adsorption energy from −1.98 eV to −1.88 eV (to −1.91 eV if the first CO_{ad} was located on a bridge site), *i.e.*, a change by 0.1 eV or less. The two CO_{ad} are located on top of the two Pt surface atoms, with a slight outwards tilt to reduce repulsions. Occupation of mixed PtAg bridge sites or even $PtAg_2$ threefold hollow sites is unfavorable. Very similar trends were obtained also when using RPBE/PBA.

Also for CO adsorption on compact Pt_3 trimers (Fig. 3), adsorption of a single CO on different sites of the trimer (on-top, bridge or threefold hollow) results in very small differences of the adsorption energy by at most 30 meV. Interestingly, for adsorption on the less symmetric on-top and bridge sites, there is a small tilt off from the vertical configuration towards the other Pt atom(s), indicating that the respective other Pt surface atom(s) have a small effect on the adsorption geometry. Addition of a second and a third CO_{ad}, which both adsorb on on-top sites, leads to changes of the mean CO adsorption energy by about 30 meV per CO, which is very close to the changes observed previously for increasing CO adsorption on a Pt_2 dimer. The differential CO adsorption energies accordingly decay from −1.96 eV (Θ_{CO} = 1/3) *via* −1.84 eV (Θ_{CO} = 2/3) to finally 1.81 eV (Θ_{CO} = 1). Also in this case, the two CO_{ad} molecules tilt away from each other to reduce CO_{ad}–CO_{ad} repulsions.

The decrease in the adsorption energy of the first CO_{ad} on the same adsorption site with increasing size of the Pt ensemble can in principle be caused by lateral ligand effects or strain effects.[25] This will be discussed in more detail at the end of the next section.

3.3.2. CO_{ad} coverage effects and CO_{ad}–CO_{ad} interactions on larger Pt_n ensembles. To mimic larger ensembles, we used linear stripes of 3 or 6 Pt atoms per 3 × 3 unit cell, which represent infinitely long strings or double strings of Pt surface atoms along the ⟨110⟩ direction, separated by 1 or 2 strings of Ag surface atoms (Fig. 4 and 5). These strings were populated with a stepwise increasing number of adsorbed CO molecules. Starting with a single CO_{ad} per unit cell on a single string of Pt atoms (Fig. 4), there is little difference in the adsorption energies between on-top adsorption and adsorption on a bridge site. This closely resembles our findings for CO adsorption on a Pt_2 dimer, where the difference in adsorption energy (on-top or bridge) was equally small. The adsorption energies are slightly lower than on the Pt_2 dimer, in full agreement with a decay in the Ag induced stabilization of the Pt–CO bond discussed in the previous section. Addition of a second CO_{ad} molecule results in a slightly lower (mean) adsorption energy, independent of whether the two molecules are adsorbed on on-top sites or on bridge sites. Again, the effective repulsion is more obvious when using the differential adsorption energy, which decreases from −1.93 eV (−1.95 eV for bridge bonded CO_{ad}) to −1.83 eV (−1.79 eV for bridge bonded CO_{ad}). Here we notice also a slight outwards tilt of the CO_{ad} molecules along the ⟨110⟩ direction to reduce the mutual repulsions. Finally, adding a third CO_{ad} results in a more significant decrease in the (mean) adsorption energy to −1.67 eV (−1.66 eV), independent of the adsorption site, which corresponds to a rather strong decrease of the differential adsorption energy from −1.83 eV (−1.79 eV) to −1.25 eV (−1.24 eV). In addition to electronic effects, this decrease in adsorption energy is partly caused by the fact that the CO_{ad}

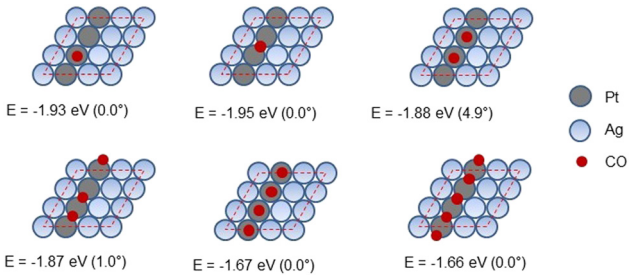

Fig. 4 Schematic representation of increasing CO adsorption on a string of Pt surface atoms in a PtAg/Pt(111) monolayer surface alloy along a close-packed ⟨110⟩ direction, both for on-top adsorption and for adsorption on bridge sites (energies in eV per molecule, angles refer to the tilt of the CO molecules with respect to the surface normal (see the text), for further details see the figure). Energies are calculated *via* PBE/PAW, and values obtained *via* RPBE/PAW are listed in the ESI† in Table S4.

molecules can no longer reduce direct repulsions by tilting away from each other along the string direction. Instead, repulsions could be reduced only by zig-zag type outwards tilts, away from the Pt string, as observed, *e.g.*, in the 2 × 1 structures of CO on Ni(110) and Pd(110).[63,64] Unfortunately, within the symmetry and size of a 3 × 3 cell it was not possible to model these kinds of tilts.

Similar calculations were also performed for a double string of Pt surface atoms (Fig. 5). Starting with a single CO_{ad} per double string, we find a further slight destabilization of the Pt–CO bond as compared to CO adsorption on the single string of Pt atoms, independent of the adsorption site. This fully agrees with the explanation of dominant Ag-induced lateral ligand effects, where replacement of a neighboring Ag surface atom by a Pt atom destabilizes the Pt–CO bond. As before, the differences between different adsorption sites are very small, with adsorption on on-top sites or bridge sites along the row (closest to the Ag atoms) being most favorable. Adding a second CO_{ad} leads to a slight lowering of the mean adsorption energy, by about 0.05 eV when comparing with the equivalent on-top configuration for a single CO_{ad}. Only when adding two more CO_{ad} species do we find a more significant weakening of the Pt–CO bond, with mean bond strengths of −1.74 eV and −1.72 eV, which is somewhere between the bond strengths obtained for 2 and 3 CO_{ad} on the single string of Pt surface atoms ($E_{ad,diff}$ around −1.60 eV). In the configurations with CO_{ad} on nearest-neighbor sites, this is accompanied also by a significant tilt of the CO_{ad} away from each other to reduce steric repulsions. Correspondingly, we expect a mean Pt–CO bond strength below −1.65 eV when saturating the double string of Pt atoms by 6 CO_{ad}, and a significantly lower value of $E_{ad,diff}$. In total, these calculations indicate that even on these larger Pt ensembles coverages up to 1 CO_{ad} per Pt surface atom are possible, as they still allow stabilization of all sites by neighboring Ag surface atoms and lowering of the repulsions by tilting.

In combination with the results reported previously for the low-coverage CO adsorption on Pt_xAg_{1-x}/Pt(111),[25] these data demonstrate that ensemble effects do not play a significant role in these systems, as the CO adsorption energy hardly changes for CO adsorption on Pt_1 monomers, Pt_2 dimers or compact Pt_3 trimers. Secondly, furthermore, CO_{ad} coverage effects seem to have little effect. Changes in the CO adsorption energy with increasing coverages, up to a local coverage of Θ_{CO} = 1, are very small, at least for small Pt_n ensembles. Hence, the effective CO_{ad}–CO_{ad} interactions must be small. This agrees perfectly with previous experimental findings from temperature programmed desorption experiments where peak broadening with increasing coverage was rather small,[25] and also from equilibrium measurements.[34] Thirdly, the fact that CO adsorption on these pseudomorphic Pt_n ensembles embedded in a matrix of Ag surface atoms is significantly stronger than adsorption on

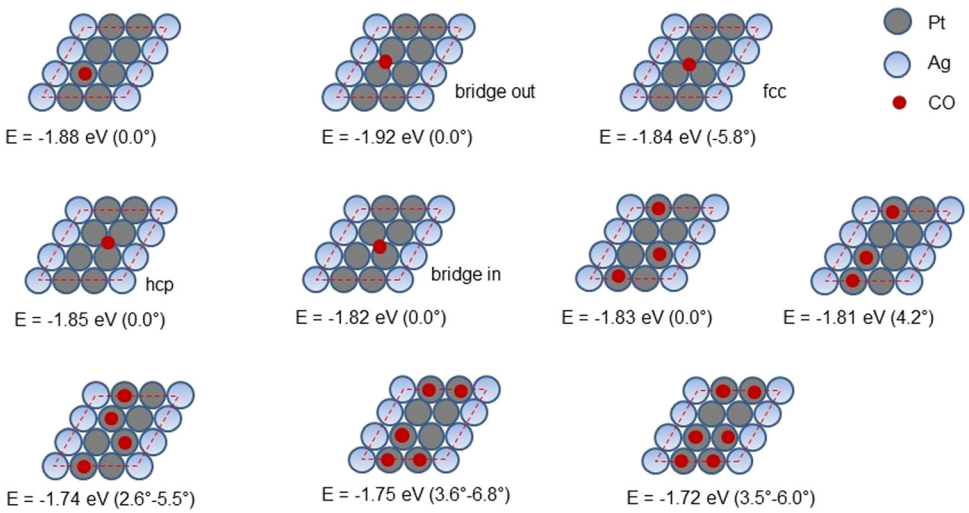

Fig. 5 Schematic representation of increasing CO adsorption on a double string of Pt surface atoms on a PtAg/Pt(111) monolayer surface alloy along a close-packed ⟨110⟩ direction, both for on-top adsorption and for adsorption on bridge sites (energies in eV per molecule, angles refer to the tilt of the CO molecules with respect to the surface normal (see the text), for further details see the figure). Energies are calculated *via* PBE/PAW, and values obtained *via* RPBE/PAW are listed in the ESI† in Table S4.

Pt(111), indicates that adsorption on Pt atoms in the surface alloy is dominated by lateral ligand effects rather than strain effects. In the present case of a pseudomorphic overlayer, we expect compressive strain induced by the larger Ag surface atoms, which would lead to a destabilization of the Pt–CO bond.[11] Such compression is indeed observed in the calculations, which show a decrease of the Pt–Pt surface bond from 2.81 Å for Pt(111) to 2.71 Å in the Pt_2 dimer in Pt_2Ag_7/Pt(111) and in the hcp Pt_3 ensemble in Pt_3Ag_6/Pt(111) (2.73 Å in the fcc Pt_3 ensemble). This destabilization is apparently overcompensated by lateral ligand effects, where the weaker Pt–Ag bonding compared to Pt–Pt results in a stabilization of the Pt–CO bond.[65] Considering the increase in bond strength when going from CO adsorption on Pt(111) to CO adsorption on individual Pt surface atoms or small ensembles (Pt_2, Pt_3) in Pt_xAg_{1-x}/Pt(111) surface alloys, ligand effects must be dominant in this system. In absolute terms, however, these changes are rather small. This also fits well with the trend observed experimentally, where the shifts in the desorption temperature with increasing CO_{ad} coverage are rather small.[25,34]

Finally, we compare these results with similar ones obtained for CO adsorption on Pd_xAg_{1-x}/Pd(111) surface alloys.[23] First of all, changes in the electronic properties of the Pd surface atoms with increasing Pd_n ensemble size are very small, much smaller than for Pt_n, as indicated by the small shift in d-band center.[23] On the other hand, CO adsorption on PdAg/Pd(111) surface alloys shows much more pronounced shifts in the adsorption energy for increasing CO_{ad} population of the Pd_n ensembles, while changes in the calculated CO adsorption energies for the same site are small. The wide range in adsorption energies is reflected also by the considerable width of the CO desorption peaks in TPD measurements.[20] The apparent discrepancy between these findings can be explained by pronounced ensemble effects on Pd-containing surfaces, which result in a significant increase in Pd–CO bond strength when changing from on-top adsorption on Pd_1 monomers (−1.37 eV), which dominates at lowest Pd concentrations, to bridge site adsorption on Pd_2 dimers (−1.64 eV), which becomes more dominant upon increasing Pd concentration, to finally adsorption on threefold hollow sites on compact Pt_3 trimers and larger ensembles (−1.97 eV), which is the dominant site at higher Pd surface concentrations.[20,23] This spread is in complete contrast to the negligible changes in adsorption energies observed on PtAg/Pt(111) monolayer surface alloys. Furthermore, for larger ensembles, adsorbate–adsorbate repulsions also play a role, while for small ensembles the displacement of adsorbed CO molecules by post-adsorbing CO molecules on less favorable adsorption sites, *e.g.*, the replacement of a more strongly bound bridge-bonded CO_{ad} on a Pd_2 dimer by two less strongly bound CO_{ad} on on-top sites, can become important. Such effects are much more pronounced for small Pd_n ensembles than for small Pt_n ensembles (see Fig. 3). The discrepancy between CO adsorption on these two monolayer surface alloys fits well to the trends observed for CO adsorption on Pd(111) and Pt(111): while for Pd(111) CO adsorption on bridge and threefold sites is strongest,[66] CO adsorption on Pt(111) is dominated by adsorption on on-top and bridge sites.[67–69] Furthermore, adsorption on Pd(111) also exhibits pronounced repulsive interactions, as indicated by the very broad TPD peaks at high coverages,[66] while this is much less the case for CO desorption on Pt(111).[39,40]

3.3.3. Multicarbonyl formation and proximity effects on Pt_xAg_{1-x}/Pt(111) surface alloys. The formation of multicarbonyl species with more than one CO_{ad} per active Pt atom was investigated for a Pt_1Ag_8/Pt(111) surface alloy. Such kind of multicarbonyl species has been reported for numerous metals,[70,71] mainly in catalysis studies performed under ambient conditions. They were often proposed to form on undercoordinated sites such as edge or corner sites on metal nanoparticles, where steric repulsion between these species can be reduced, in addition to the generally stronger binding of adsorbates on these sites.[65]

Repulsion between closely neighbored CO_{ad} species can also be reduced for adsorption on individual active surface atoms or small ensembles of surface atoms embedded in a matrix of inert surface atoms. In the present surface alloys, Pt surface atoms in a Pt_1Ag_8/Pt(111) surface alloy would be the most simple example (see Fig. 6). For the first CO_{ad} the on-top site with a vertical CO_{ad} is the most stable adsorption site and configuration. Adding a second CO_{ad}, the most stable configuration involves adsorption on two bridge sites or threefold-hollow sites opposite from each other on both sides of the active Pt atom. For adsorption on threefold-hollow sites this must include one fcc and one hcp site, respectively. In both cases the CO_{ad} are significantly tilted, by about 17° with respect to the surface normal away from each other, to increase the separation between the two molecules, in particular between the two O atoms. Using PBE/PAW, the adsorption energy (per CO_{ad} molecule) decreases from 2.06 eV to 1.04 eV. The drastic decrease in adsorption energy is even more obvious when using the differential adsorption energy $E_{ad,diff}$, which for the addition of a second CO_{ad} molecule is only 0.02 eV. With this low value, the formation of multicarbonyl species on these sites can be excluded at finite temperatures, even though these Pt_1 sites are more strongly binding than Pt atoms on Pt(111) and even though the CO_{ad} molecules can reduce the CO_{ad}–CO_{ad} repulsion by a significant tilt. This agrees with the experimental situation in so far as the formation of multicarbonyl species has rarely been proposed for Pt nanoparticle catalysts,[41,42] in contrast, *e.g.*, to multicarbonyl formation on Ru nanoparticles.[71–73] Finally, we would like to note that this conclusion is purely based on the calculated adsorption energy, *i.e.*, it does not

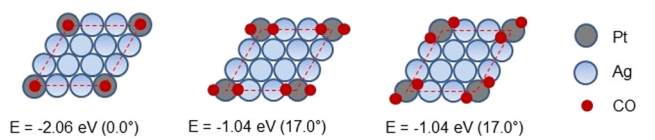

Fig. 6 CO adsorption on Pt_1 in Pt_1Ag_8/Pt(111) (energies in eV per molecule, angles refer to the tilt of the CO molecules with respect to the surface normal (see the text), for further details see the figure). Energies are calculated *via* PBE/PAW, and values obtained *via* RPBE/PAW are listed in the ESI† in Table S4.

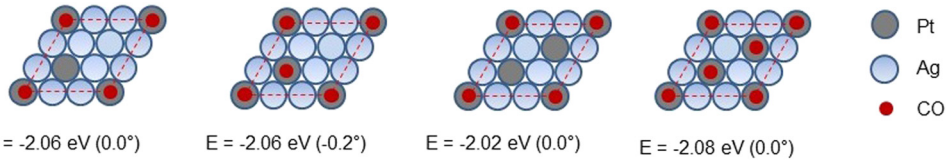

Fig. 7 CO adsorption on separated Pt_1 monomers in Pt_2Ag_7/Pt(111) and Pt_3Ag_6/Pt(111) surface alloys along the ⟨210⟩ direction (energies in eV per molecule, angles refer to the tilt of the CO molecules with respect to the surface normal (see the text), for further details see the figure). Energies are calculated *via* PBE/PAW, and values obtained *via* RPBE/PAW are listed in the ESI† in Table S4.

include kinetic barriers, and is specific for the given configuration. Nevertheless, it clearly indicates that even in the absence of closely neighbored CO adspecies binding of more than one CO to an individual Pt surface atom is essentially inhibited on flat surfaces.

As a last point we explored proximity effects, *i.e.*, the effective interaction between CO_{ad} molecules adsorbed on two active surface atoms which are not directly neighbored, but also not very distant. This was modelled by CO adsorption on two separated Pt_1 monomers, as illustrated in Fig. 7. Note that this configuration with two next-nearest neighbor Pt surface atoms along the ⟨210⟩ direction represents the one with the closest Pt–Pt possible for non-neighbored surface atoms. Starting with adsorption of a single CO on one of the two Pt surface atoms in Fig. 7 (left), we find that electronic Pt–Pt interactions do not affect the CO adsorption energy on one of these Pt surface atoms. With 2.06 eV it is identical to that obtained for adsorption on a Pt_1 monomer in a Pt_1Ag_8/Pt(111) unit cell (Fig. 6). Furthermore, adsorption of a second CO on the second Pt_1 monomer has no measurable effect on the CO adsorption energy. The only difference is a very small tilt of the two CO_{ad}, both pointing with the same orientation along the close-packed ⟨210⟩ direction, most likely due to the surrounding non-symmetric atom distribution rather than by mutual repulsions or attractions. Apparently, these kinds of proximity effects are negligible for the present system. This also fits well with the observation of rather small effects (∼50 meV per CO_{ad}) for adsorption of 2 CO on neighboring Pt surface atoms in a Pt_2 dimer (Fig. 3).

Going to higher coverages of non-neighbored Pt surface atoms, which is illustrated for 3 Pt surface atoms per unit cell in Fig. 7, we again find small effects from effective Pt–Pt interactions. This is indicated by the further decrease of the adsorption energy of the first CO to −2.02 eV, while in the previous case (adsorption on two Pt monomers) this remained at −2.06 eV. Most simply, the lower CO adsorption energy can be explained by a lower contribution from stabilizing (longer-range) ligand-plus-strain effects, due to replacement of a larger Ag surface atom by Pt. Additional adsorption of two further CO on the remaining two Pt surface atoms results in an increase of the mean CO adsorption energy to −2.08 eV per CO_{ad}. This corresponds to an increase in the differential adsorption energy to −2.11 eV per CO_{ad} for the 2nd and 3rd CO_{ad}. Different from the previous case of two Pt_1 monomers in the 3 × 3 unit cell there is no measurable tilt of the CO_{ad}. Most simply, the absence of a tilt is caused by the presence of two neighboring CO, whose effects compensate each other. For the increase in adsorption energy, which differs from the previous cases investigated here and which despite its small size is significant, we speculate that this is due to attractive through-bond interactions, which overcompensate repulsive direct interactions.

The results presented in this section first of all indicate that there is no driving force for the formation of multicarbonyl species on these PtAg/Pt(111) surface alloys, which seems to be valid also in more general for Pt nanoparticles. Second, proximity effects, indicating interactions between CO_{ad} molecules adsorbed on non-neighbored Pt surface atoms, *i.e.*, Pt surface atoms that are separated by at least one inert surface atom, seem to be negligible or very small for this system.

4. Conclusions

Using periodic density functional theory calculations and extending our previous combined experimental and theoretical work,[25] we could provide detailed insights on the stability, electronic properties and CO adsorption behavior of pseudomorphic bimetallic PtAg surfaces supported on a Pt(111) substrate. These include surfaces covered by pseudomorphic Ag film of 1–3 layers in thickness, Pt(111) layers with one or two Ag layers underneath, and monolayer PtAg surface alloys, either on Pt(111) or with 1 or 2 Ag layers underneath and then Pt(111). In addition to finding that Ag segregation is always favorable compared with Ag underlayer formation, and intermixing into surface alloys is more favorable than separation into Ag and Pt surface phases, the data provide quantitative information on the stability of different surface configurations. Calculations of the LDOS on the Pt surface atoms in the monolayer surface alloy reveal an increasing up-shift of the d-band center with increasing number of neighboring Ag surface atoms. Furthermore, they show a decoupling of the Pt surface atoms from the bulk in a Pt_1Ag_8/Pt(111) monolayer surface alloy in the case of Ag underlayers beneath, with a dominant state about 1.5 eV below the Fermi level.

Systematic evaluation of the CO adsorption properties on various different Pt_n ensembles (n = 1–3) in a matrix of Ag surface atoms reveal very small changes in the adsorption energy with increasing number of CO_{ad} on the ensemble, up to 1 CO_{ad} per Pt surface atom. Furthermore, the differences between different adsorption sites for CO on Pt_2 dimers and compact Pt_3 trimers are very small. On the other hand, the data show a weak, but clear increase of the adsorption energy on Pt with increasing number of neighboring Ag surface atoms, which is explained by dominant electronic ligand effects. The results are consistent with experimental findings of rather

narrow desorption peaks and the (coverage dependent) occupation of different adsorption sites.

The formation of multicarbonyl species, with two CO binding to a single, individual Pt surface atom, can be excluded at finite temperatures. With a differential adsorption energy of 0.02 eV, the second CO_{ad} is too weakly bound to be populated under these conditions, in good agreement with experimental findings for supported Pt nanoparticles. Despite the stronger adsorption on the $PtAg_6$ site and despite the possibility of lowering the CO_{ad}–CO_{ad} repulsions by tilting the molecules away from each other, the effective repulsions, both by direct repulsion and by indirect electronic effects, are too strong to facilitate multicarbonyl formation. On the other hand, proximity effects, reflecting interactions between CO_{ad} on two Pt surface atoms separated by at least one Ag surface atom, were found to be negligible, consistent with the result that even for $2CO_{ad}$ on a Pt_2 dimer the effective interaction is negligible. Overall, the interactions between CO_{ad} species on small Pt_n ensembles (n = 1–3) and also on one-dimensional Pt strings in PtAg/Pt(111) surface alloys seem to be very weak.

Finally, a more general understanding of bimetallic surface properties was obtained by systematic comparison with similar data obtained previously for bimetallic PdAg/Pd(111) and Ag/Pd(111) surfaces, which despite their close structural similarity exhibit characteristic differences in their stability, electronic properties and CO adsorption behavior. The results derived in this model study provide detailed insights into the chemistry of bimetallic PtAg surfaces, which is also useful for a better understanding and possible improvement in the performance of bimetallic PtAg catalysts.

Conflicts of interest

There are no conflicts of interest to declare.

Acknowledgements

This work was supported by the Baden-Württemberg Stiftung through the Competence Network for Functional Nanostructures (project 'Clean Tech'). Computational resources were provided by the JUSTUS high-performance computing facility at Ulm University as part of the bwHPC initiative of the Federal State of Baden-Württemberg.

References

1 G.-M. Schwab, Alloy Catalysts in Dehydrogenation, *Discuss. Faraday Soc.*, 1950, **8**, 166–171.
2 D. A. Dowden and P. W. Reynolds, Some Reactions over Alloy Catalysts, *Discuss. Faraday Soc.*, 1950, **8**, 184.
3 J. H. Sinfelt, Catalysis by Alloys and Bimetallic Clusters, *Acc. Chem. Res.*, 1977, **10**, 15–20.
4 W. M. H. Sachtler and R. A. van Santen, Surface Composition and Selectivity of Binary Alloys, *Adv. Catal.*, 1977, **26**, 69–119.
5 V. Ponec, Alloy Catalysts: the Concept, *Appl. Catal., A*, 2001, **222**, 31–45.
6 J. H. Sinfelt, Role of Surface Science in Catalysis, *Surf. Sci.*, 2002, **500**, 923–946.
7 Y. Soma-Noto and W. M. H. Sachtler, Infrared Spectra of Carbon Monoxide Adsorbed on Supported Palladium and Palladium-Silver Alloys, *J. Catal.*, 1974, **32**, 315–324.
8 J. W. A. Sachtler and G. A. Somorjai, Influence of Ensemble Size on CO Chemisorption and Catalytic N-Hexane Conversion by Au-Pt(111) Bimetallic Single-Crystal Surfaces, *J. Catal.*, 1983, **81**, 77–94.
9 V. Ponec and W. M. H. Sachtler, The Reactions Between Cyclopentane and Deuterium on Nickel and Nickel-Copper Alloys, *J. Catal.*, 1972, **24**, 250–261.
10 Y. L. Lam, J. Criado and M. Boudart, Enhancement by Inactive Gold of the Rate of the H_2–O_2 Reaction on Active Palladium: A Ligand Effect, *Nouv. J. Chim.*, 1977, **1**, 461.
11 M. Mavrikakis, B. Hammer and J. K. Nørskov, Effect of Strain on the Reactivity of Metal Surfaces, *Phys. Rev. Lett.*, 1998, **81**, 2819–2822.
12 B. Hammer and J. K. Nørskov, Theoretical Surface Science and Catalysis – Calculations and Concepts, *Adv. Catal.*, 2000, **45**, 71–129.
13 A. Groß, Reactivity of Bimetallic Systems Studied From First Principles, *Top. Catal.*, 2006, **37**, 29–40.
14 J. T. Yates, C. H. F. Peden and D. W. Goodman, Copper Site Blocking of Hydrogen Chemisorption on Ruthenium, *J. Catal.*, 1985, **94**, 576–580.
15 R. G. Windham, B. E. Koel and M. T. Paffett, Studies of the Ensemble Size Requirements for Ethylene Adsorption and Decomposition on Platinum(111): Ethylene and Bismuth Coadsorption, *Langmuir*, 1988, **4**, 1113–1118.
16 C. Xu and B. E. Koel, Probing the Modifier Precursor State: Adsorption of CO on Sn/Pt(111) Surface Alloys, *Surf. Sci.*, 1994, **304**, L505–L511.
17 S. Sakong, C. Mosch and A. Groß, CO Adsorption on Cu-Pd Alloy Surfaces: Ligand Versus Ensemble Effects, *Phys. Chem. Chem. Phys.*, 2007, **9**, 2216–2225.
18 L. A. Mancera, T. Diemant, A. Groß and R. J. Behm, Molecular and Dissociative Hydrogen Adsorption on Bimetallic PdAg/Pd(111) Surface Alloys: A Combined Experimental and Theoretical Study, *J. Phys. Chem. C*, 2022, **126**, 3060–3077.
19 Y. Ma, J. Bansmann, T. Diemant and R. J. Behm, Formation, Stability and CO Adsorption Properties of PdAg/Pd(111) Surface Alloys, *Surf. Sci.*, 2009, **603**, 1046–1054.
20 Y. Ma, T. Diemant, J. Bansmann and R. J. Behm, The Interaction of CO With PdAg/Pd(111) Surface Alloys – A Case Study of Ensemble Effects on a Bimetallic Surface, *Phys. Chem. Chem. Phys.*, 2011, **13**, 10741–10754.
21 A. K. Engstfeld, H. E. Hoster and R. J. Behm, Formation, Atomic Distribution and Mixing Energy in Two-Dimensional Ag_xPd_{1-x} Surface Alloys on Pd(111), *Phys. Chem. Chem. Phys.*, 2012, **14**, 10754–10761.
22 A. P. Farkas, T. Diemant, J. Bansmann and R. J. Behm, The Adsorption of Oxygen and Coadsorption of CO and Oxygen on PdAg/Pd(111) Surface Alloys, *Chem. Phys. Chem.*, 2012, **13**, 3516–3525.

23 L. A. Mancera, R. J. Behm and A. Groß, Structure and Local Reactivity of PdAg/Pd(111) Surface Alloys, *Phys. Chem. Chem. Phys.*, 2013, **15**, 1497–1508.
24 T. Diemant, K. M. Schüttler and R. J. Behm, Ag on Pt(111): Changes in Electronic and CO Adsorption Properties Upon PtAg/Pt(111) Monolayer Surface Alloy Formation, *Chem. Phys. Chem.*, 2015, **16**, 2943–2952.
25 K. M. Schüttler, L. A. Mancera, T. Diemant, A. Groß and R. J. Behm, Interaction of CO With Pt_xAg_{1-x}/Pt(111) Surface Alloys: More than Dilution by Ag Atoms, *Surf. Sci.*, 2016, **650**, 237–254.
26 S. Beckord, A. K. Engstfeld, S. Brimaud and R. J. Behm, Electrochemical Characterization and Stability of Ag_xPt_{1-x}/Pt(111) Surface Alloys, *J. Phys. Chem. C*, 2016, **120**, 16179–16190.
27 S. Beckord, S. Brimaud and R. J. Behm, Stability and ORR Performance of a Well-Defined Bimetallic $Ag_{70}Pt_{30}$/Pt(111) Monolayer Surface Alloy Electrode – Probing the De-Alloying at an Atomic Scale, *Electrochim. Acta*, 2018, **259**, 762–771.
28 S. Beckord, S. Brimaud and R. J. Behm, The Performance of Structurally Well-Defined Ag_xPt_{1-x}/Pt(111) Surface Alloys in the Oxygen Reduction Reaction-An Atomic-Scale Picture, *J. Electroanal. Chem.*, 2018, **819**, 401–409.
29 H. Röder, R. Schuster, H. Brune and K. Kern, Monolayer-Confined Mixing at the Ag–Pt(111) Interface, *Phys. Rev. Lett.*, 1993, **71**, 2086–2089.
30 U. Strüber and J. Küppers, Spectroscopic Confirmation of STM Derived Ag/Pt Mixing in Annealed Ag Submonolayers at Pt(111) Surfaces, *Surf. Sci.*, 1993, **294**, L924–L928.
31 T. Härtel, U. Strüber and J. Küppers, Growth and Properties of Thin Ag Films on Pt(111) Surfaces, *Thin Solid Films*, 1993, **229**, 163–170.
32 J. S. Tsay, Y. D. Yao and C. S. Shern, Dynamic Study of a Surface-Confined Alloy in Ultrathin Ag/Pt(111) Film, *Phys. Rev. B: Condens. Matter Mater. Phys.*, 1998, **58**, 3609–3612.
33 M. Jankowski, E. van Vroonhoven, H. Wormeester, H. J. W. Zandvliet and B. Poelsema, Alloying, Dealloying, and Reentrant Alloying in (Sub)Monolayer Growth of Ag on Pt(111), *J. Phys. Chem. C*, 2017, **121**, 8353–8363.
34 U. Bauer, F. Späth, F. Düll, P. Bachmann, J. Steinhauer, H. P. Steinrück and C. Papp, Reactivity of CO and C_2H_4 on Bimetallic Pt_xAg_{1-x}/Pt(111) Surface Alloys Investigated by High-Resolution X-Ray Photoelectron Spectroscopy, *Chem. Phys. Chem.*, 2018, **19**, 1432–1440.
35 M. Hua, X. Tian, S. Li, A. Shao and X. Lin, Theoretical Design of Platinum-Silver Single Atom Alloy Catalysts With CO Adsorbate-Induced Surface Structures, *Phys. Chem. Chem. Phys.*, 2022, **24**, 19488–19501.
36 F. M. Cuevas-Muñiz, M. P. Gurrola, O. Téllez-Vázquez, R. Esparza, M. Guerra-Balcázar, L. G. Arriaga and J. Ledesma-García, Correlation Between Theoretical Data and Experimental Selective Properties of PtAg Core-Shell Nanoparticles for Oxygen Reduction Reactions, *Int. J. Hydrogen Energy*, 2015, **40**, 17284–17290.
37 V. V. Pryadchenko, V. V. Srabionyan, E. B. Mikheykina, L. A. Avakyan, V. Y. Murzin, Y. V. Zubavichus, I. Zizak, V. E. Guterman and L. A. Bugaev, Atomic Structure of Bimetallic Nanoparticles in PtAg/C Catalysts: Determination of Components Distribution in the Range From Disordered Alloys to ''Core–Shell'' Structures, *J. Phys. Chem. C*, 2015, **119**, 3217–3227.
38 X. Weng, Q. Liu, A. J. Wang, J. Yuan and J. J. Feng, Simple One-Pot Synthesis of Solid-Core@Porous-Shell Alloyed PtAg Nanocrystals for the Superior Catalytic Activity Toward Hydrogen Evolution and Glycerol Oxidation, *J. Colloid Interface Sci.*, 2017, **494**, 15–21.
39 G. Ertl, M. Neumann and K. M. Streit, Chemisorption of CO on the Pt(111) Surface, *Surf. Sci.*, 1977, **64**, 393–410.
40 P. R. Norton, J. W. Goodale and E. B. Selkirk, Adsorption of CO on Pt(111) Studied by Photoemission, Thermal Desorption Spectroscopy and High Resolution Dynamic Measurements of Work Function, *Surf. Sci.*, 1979, **83**, 189–227.
41 S. C. Tsang, N. Cailuo, W. Oduro, A. T. S. Kong, L. Clifton, K. M. K. Yu, B. Thiebaut, J. Cookson and P. Bishop, Engineering Preformed Cobalt-Doped Platinum Nanocatalysts for Ultraselective Hydrogenation, *ACS Nano*, 2008, **2**, 2547–2553.
42 W. O. Oduro, N. Cailuo, K. M. Yu, H. Yang and S. C. Tsang, Geometric and Electronic Effects on Hydrogenation of Cinnamaldehyde over Unsupported Pt-Based Nanocrystals, *Phys. Chem. Chem. Phys.*, 2011, **13**, 2590–2602.
43 G. Kresse and J. Furthmüller, Efficient Iterative Schemes for Ab Initio Total-Energy Calculations Using a Plane-Wave Basis Set, *Phys. Rev. B: Condens. Matter Mater. Phys.*, 1996, **54**, 11169–11186.
44 J. P. Perdew, K. Burke and M. Ernzerhof, Generalized Gradient Approximation Made Simple, *Phys. Rev. Lett.*, 1996, **77**, 3865–3868.
45 B. Hammer, L. B. Hansen and J. K. Nørskov, Improved Adsorption Energetics within Density-Functional Theory Using Revised Perdew-Burke-Ernzerhof Functionals, *Phys. Rev. B: Condens. Matter Mater. Phys.*, 1999, **59**, 7413–7421.
46 P. E. Blöchl, Projector Augmented-Wave Method, *Phys. Rev. B: Condens. Matter Mater. Phys.*, 1994, **50**, 17953–17979.
47 G. Kresse and D. Joubert, From Ultrasoft Pseudopotentials to the Projector Augmented-Wave Method, *Phys. Rev. B: Condens. Matter Mater. Phys.*, 1999, **59**, 1758–1775.
48 G. Kresse and J. Furthmüller, Efficiency of Ab-Initio Total Energy Calculations for Metals and Semiconductors Using a Plane-Wave Basis Set, *Comput. Mater. Sci.*, 1996, **6**, 15–50.
49 R. A. L. P. Wyckoff, *Crystal Structures*, Interscience Publ., New York, 1963, vol. 1.
50 D. Mahlberg, S. Sakong, K. Forster-Tonigold and A. Groß, Improved DFT Adsorption Energies with Semiempirical Dispersion Corrections, *J. Chem. Theory Comput.*, 2019, **15**, 3250–3259.
51 S. V. Barabash, V. Blum, S. Müller and A. Zunger, Prediction of Unusual Stable Ordered Structures of Au–Pd Alloys Via First-Principles Cluster Expansion, *Phys. Rev. B: Condens. Matter Mater. Phys.*, 2006, **74**, 035108.
52 H. Brune, H. Röder, C. Boragno and K. Kern, Strain Relief at Hexagonal-Close-Packed Interfaces, *Phys. Rev. B: Condens. Matter Mater. Phys.*, 1994, **49**, 2997–3000.

53 G. Rangelov, T. Fauster, U. Strüber and J. Küppers, Stacking of Ag Layers on Pt(111), *Surf. Sci.*, 1995, **331–333**, 948–951.
54 B. Hammer, Special Sites at Noble and Late Transition Metal Catalysts, *Top. Catal.*, 2006, **37**, 3–16.
55 A. Groß, Tailoring the Reactivity of Bimetallic Overlayer and Surface Alloy Systems, *J. Phys.: Condens. Matter*, 2009, **21**, 084205.
56 B. Hammer, O. H. Nielsen and J. K. Nørskov, Structure Sensitivity in Adsorption: CO Interaction With Stepped and Reconstructed Pt Surfaces, *Catal. Lett.*, 1997, **46**, 31–35.
57 J. K. Nørskov, J. Rossmeisl, A. Logadottir, L. Lindqvist, J. R. Kitchin, T. Bligaard and H. Jónsson, Origin of the Overpotential for Oxygen Reduction at a Fuel-Cell Cathode, *J. Phys. Chem. B*, 2004, **108**, 17886–17892.
58 A. K. Henß, S. Sakong, P. K. Messer, J. Wiechers, R. Schuster, D. C. Lamb, A. Groß and J. Wintterlin, Density Fluctuations As Door-Opener for Diffusion on Crowded Surfaces, *Science*, 2019, **363**, 715–718.
59 J. Wei, R. Amirbeigiarab, Y. X. Chen, S. Sakong, A. Gross and O. M. Magnussen, The Dynamic Nature of CO Adlayers on Pt(111) Electrodes, *Angew. Chem., Int. Ed.*, 2020, **59**, 6182–6186.
60 M. Ruff, N. Takehiro, P. Liu, J. K. Nørskov and R. J. Behm, Size-Specific Chemistry on Bimetallic Surfaces: A Combined Experimental and Theoretical Study, *Chem. Phys. Chem.*, 2007, **8**, 2068–2071.
61 M. S. Chen, K. Luo, T. Wei, Z. Yan, D. Kumar, C. W. Yi and D. W. Goodman, The Nature of the Active Sites for Vinyl Acetate Synthesis Over Pd-Au, *Catal. Today*, 2006, **117**, 37–45.
62 M. Chen and D. W. Goodman, Promotional Effects of Au in Pd-Au Catalysts for Vinyl Acetate Synthesis, *Chin. J. Catal.*, 2008, **29**, 1178–1186.
63 R. J. Behm, G. Ertl and V. Penka, Adlayer Geometry and Structural Effects in the CO/Ni(110) System, *Surf. Sci.*, 1985, **160**, 387–399.
64 D. Rieger, R. D. Schnell and W. Steinmann, Angular Distribution Patterns of Photoelectrons from Orbitals of CO Adsorbed on Ni(100), Pt(111) and Pt(110), *Surf. Sci.*, 1984, **143**, 157–176.
65 B. Hammer, Y. Morikawa and J. K. Nørskov, CO Chemisorption at Metal Surfaces and Overlayers, *Phys. Rev. Lett.*, 1996, **76**, 2141–2144.
66 J. Szanyi, W. K. Kuhn and D. W. Goodman, CO Adsorption on Pd(111) and Pd(100): Low and High Pressure Correlations, *J. Vac. Sci. Technol. A*, 1993, **11**, 1969–1974.
67 J. C. Campuzano, in *The Chemical Physisc of Solid Surfaces and Heterogeneous Catalysis*, ed. D. A. King and D. P. Woodruff, Elsevier Publishers, Amsterdam, 1990, vol. 3A, pp. 389–470.
68 B. Shan, Y. Zhao, J. Hyun, N. Kapur, J. B. Nicholas and K. Cho, Coverage-Dependent CO Adsorption Energy From First-Principles Calculations, *J. Phys. Chem. C*, 2009, **113**, 6088–6092.
69 G. T. K. Gunasooriya and M. Saeys, CO Adsorption on Pt(111): From Isolated Molecules to Ordered High-Coverage Structures, *ACS Catal.*, 2018, **8**, 10225–10233.
70 T. M. Duncan, K. W. Zilm, D. M. Hamilton and T. W. Root, Adsorbed States of Carbon Monoxide on Dispersed Metals: a High-Resolution Solid-State NMR Study, *J. Phys. Chem.*, 1989, **93**, 2583–2590.
71 S. Y. Chin, C. T. Willimas and M. D. Amiridis, FTIR Studies of CO Adsorption on Al_2O_3- and SiO_2-Supported Ru Catalysts, *J. Phys. Chem. B*, 2006, **110**, 871–882.
72 B. T. Loveless, C. Buda, M. Neurock and E. Iglesia, CO Chemisorption and Dissociation at High Coverages During CO Hydrogenation on Ru Catalysts, *J. Am. Chem. Soc.*, 2013, **135**, 6107–6121.
73 Y. Yan, Q. Wang, C. Jiang, Y. Yao, D. Lu, J. Zheng, Y. Dai, H. Wang and Y. Yang, Ru/Al_2O_3 Catalyzed CO_2 Hydrogenation: Oxygen-Exchange on Metal-Support Interfaces, *J. Catal.*, 2018, **367**, 194–205.